Surv Geophys (2016) 37:81–107
DOI 10.1007/s10712-015-9334-2

On the Coupling of Geodynamic and Resistivity Models: A Progress Report and the Way Forward

Wiebke Heise[1] · **Susan Ellis**[1]

Received: 30 October 2014 / Accepted: 31 July 2015 / Published online: 12 August 2015

Abstract Magnetotelluric (MT) studies represent the structure of crust and mantle in terms of conductivity anomalies, while geodynamic modelling predicts the deformation and evolution of crust and mantle subject to plate tectonic processes. Here, we review the first attempts to link MT models with geodynamic models. An integration of MT with geodynamic modelling requires the use of relationships between conductivity and rheological parameters such as viscosity and melt fraction, which are provided by laboratory measurements of rock properties. Owing to present limitations in our understanding of these relationships, and in interpreting the trade-off between scale and magnitude of conductivity anomalies from MT inversions, most studies linking MT and geodynamic models are qualitative rather than providing hard constraints. Some recent examples attempt a more quantitative comparison, such as a study from the Himalayan continental collision zone, where rheological parameters have been calculated from a resistivity model and compared to predictions from geodynamic modelling. We conclude by demonstrating the potential in combining MT results and geodynamic modelling with examples that directly use MT results as constraints within geodynamic models of ore bodies and studies of an active volcano-tectonic rift.

Keywords Numerical modelling · Magnetotellurics · Partial melt · Geodynamics

1 Introduction

Geodynamic models attempt to explore, in a mechanically and geologically consistent manner, the deformation and evolution of crust and mantle subject to plate tectonic processes. They can encompass a variety of scales: both temporal (earthquake rupture

✉ Wiebke Heise
w.heise@gns.cri.nz

[1] GNS Science, PO Box 30-368, Lower Hutt 5040, New Zealand

timescales to millions of years) and physical (from microstructure to outcrop scale, and ranging up to the scale of tectonic plate interactions and mantle convection). Rather than exactly matching what we measure geologically and geophysically, the goal of geodynamic modelling is to gain insight into the principal controls on the evolution and mechanics of a particular region while keeping input parameters as simple as possible.

Numerical geodynamic modelling techniques are becoming increasingly sophisticated and are now able to explore deformation of crust and mantle with varied rock compositions, fluid content and melt fractions (e.g., Bittner and Schmeling 1995; Upton 1998; Beaumont et al. 2001; Gerya and Yuen 2003; Rey et al. 2009; Ellis et al. 2011; Gerya and Meilick 2011; Angiboust et al. 2012; Keller et al. 2013; Liu et al. 2014; Quinquis and Buiter 2014). It is desirable to constrain such models quantitatively with surface geology (such as mapped structure, faults, lithology, and thermo-chronological information) and with geophysical measurements of the subsurface (e.g., seismic and electrical structure). Using these constraints, such models can offer an integration of different datasets, providing additional insight into earth processes. Geodynamic modellers incorporate a large number of parameters that can include: elastic, frictional-plastic and ductile flow parameters relating rock composition and rheology; fluid content (both in terms of its effect on ductile flow and brittle yield via modification of yield stress); thermal parameters such as radiogenic heating and thermal conductivity (for coupled mechanical-thermal models); and melt fraction (with corresponding changes in density, heat advection and ductile strength). Models can be two- or three dimensional and have boundary conditions constrained by tectonic forcing, and heat and fluid flow at the base and surface of the model. Observations from geophysics are particularly useful in geodynamic models that have initial conditions corresponding to present-day conditions ("snapshot" models, which are used to predict present-day strain rates, temperature profiles and fluid content). They are less useful in geodynamic models considering long-term evolution over millions of years, although in these cases the final predictions from the models may be compared to present-day observations.

In contrast, geophysical models usually only resolve one parameter—in the case of electromagnetic (EM) methods, the electrical conductivity. To use such conductivity models, geodynamic modellers have to understand the limitations inherent in resolving structures with electromagnetic techniques. In this review, we will refer to both conductivity (σ [S/m]) and its inverse resistivity (ρ [Ωm]) for electrical properties of crust and mantle. We also refer to "conductance", which is the thickness conductivity product (σh [S]) of a horizontal layer. We use the term "conductor" to describe an area of higher conductivity within a more resistive background.

Here, we will focus on the magnetotelluric (MT) method, since it is the principal electromagnetic method with an investigation depth great enough to study the conductivity structure of deeper crust and mantle. The subsurface conductivity structure in magnetotelluric data is derived from (linear) frequency–domain relationships between the surface horizontal magnetic and electric field components. Depending on the frequency of the electromagnetic wave, the penetration depth of MT signals and thus the investigation depth of the magnetotelluric (MT) method vary from hundreds of metres to mantle depth. Due to the diffusive nature of the electromagnetic energy, magnetotelluric soundings resolve conductivity gradients rather than sharp contrasts. Therefore, typical inversion schemes seek the "minimum structure" model, the smoothest model that fits the data within given error levels instead of a rougher model that fits the data as well as possible. The smoothing parameters in the inversion define the trade-off between model roughness and misfit, and there will be always a variety of models (with different degrees of roughness) which fit the data to a similar degree. As a consequence of this regularization process, most MT

inversions are smooth and do not resolve sharp contrasts and conductors are often smeared to depth (for a review on inversion, see, e.g., Pek and Santos 2006; Rodi and Mackie 2012; for approaches including sharp boundaries, see e.g. Smith et al. 1999; McGary et al. 2014).

A key point to communicate to any users of MT data is that non-uniqueness of the MT method can make the interpretation of the size, geometry and depth of an anomaly ambiguous. For example, in a horizontal layered earth, inversion of MT data gives the conductance rather than the conductivity of a layer. In this case, a range of thickness–bulk conductivity combinations is possible and needs to be explored (e.g., Bahr and Simpson 2005). However, edges and topography (e.g., dip) of an anomaly contain information about its shape and therefore give some constraint on conductivity and thickness. Also, the so-called screening effect of conductors close to the surface lowers the resolution of structures below. Generally, the top of conductive structures within resistive background and lateral conductivity contrasts are well resolved but not the bottom of conductors. Artefacts or weakly resolved anomalies can also appear in inversion models in areas where data coverage is not sufficient and/or if the smoothing is not adequate (too rough). Finally, for interpreting conductivity values from a MT model it is important to note that the absolute value of conductivity might be over- or underestimated in inversion models, depending on the starting model. Siripunvaraporn and Egbert (2009) show a simple case where conductivity is overestimated using the inversion code WSINV3DMT which is widely used in the MT community.

In this paper, we give an overview of recent work that integrates MT results and numerical geodynamic models. Following this introduction of MT method and geodynamic modelling, we divide this paper into two parts, "crust" and "mantle", describing first the causes for respective conductivity anomalies, then the existing laboratory studies linking conductivity to rock properties, and finally, we present examples where conductivity models have been compared or linked to geodynamic models. We focus on the main ways in which they have been linked: where modelling has been used to help interpret what causes the MT conductivity anomaly; and where rheological parameters have been calculated from a resistivity model (e.g., crustal melting, the presence of interconnected fluids, or mantle anisotropy and viscosity) to help constrain or test the geodynamic models. As of the writing of this review, most studies attempting to integrate MT and geodynamic models are what we would class as "weak" links, i.e. they are mostly qualitative rather than providing hard constraints for each other. In the last part of our review, we attempt to point the way forward to a more quantitative integration of MT and geodynamic models.

2 Electromagnetic Methods: Providing Constraints for Geodynamic Modellers

Many good reviews are already available as resources for the geodynamic modeller wishing to constrain or test models with MT inversion results. Table 1 lists some of those that are most accessible to non-MT experts.

The temptation amongst geodynamic modellers is to relate electrical conductivity to rheological parameters used in their models (such as fluid content) without regard to the tectonic environment and history. In fact, as MT practitioners are aware, electrical conductivity can be affected by many quantities that affect rock strength and behaviour, not just fluid content. It may relate to lithology, fluid content and connectivity, presence of (interconnected) partial melt, clays, graphite or conductive minerals. The relationship between MT data and conductivity is inherently nonlinear. No simple, generalized "module" exists that can take conductivity as an input parameter and predict quantities

Table 1 Recent review papers useful for non-MT experts to use in geodynamic models

References	Topic	Comments
Unsworth and Rondenay (2013)	Mapping the distribution of fluids in the crust and lithospheric mantle utilizing geophysical methods	Summarizes main MT and seismic signatures of fluids in crust and mantle and discusses various tectonic environments
Pommier (2013)	Interpretation of MT results using laboratory measurements	Reviews main laboratory results pertaining to understanding MT profiles in crust and mantle
Pommier et al. (2013)	Prediction of silicate and basaltic melt viscosity in magma chambers from MT	Could be used as a direct input to a geodynamic model
Karato (2011)	Water content in mantle from electrical resistivity	Could be used as direct input to geodynamic model
Glover (2010)	Mixing models for electrical conductivity in porous media	Relates the conductivity of a rock to its porosity and the conductivity of the fluid

used to constrain geodynamic models such as mineral composition, elasticity, porosity and permeability, fluid type and amount, or viscosity is available, nor is it possible. Instead, MT results must be carefully interpreted on a tectonic-case basis to compare with or provide input to geodynamic models.

Finally, it is important that geodynamic modellers are aware that we do not yet have a full understanding of the dependence of conductivity on polymineralic rock composition (e.g., presence of some minerals with high conductance such as graphite) and multiple phases (e.g., interconnected conductive fluids and/or melt). The link between conductivity model and parameters that are used in geodynamic modelling is only possible using laboratory measurements, which have not yet been fully described, especially for polymineralic rocks. Once a best-fit inversion has recovered the conductivity distribution of the subsurface, laboratory measurements can help provide constraints on the conductivity of rocks at conditions that are representative for the Earth, including temperature, pressure, thermodynamic conditions, fluid content, redox conditions and texture (e.g., Pommier 2013). However, these studies are work in progress and do not always give a consistent set of relationships. An example is the recent study by Hashim et al. (2013), which conducted laboratory experiments to constrain the melt percentages in the Himalaya at pressures and temperatures relevant for lower crustal depths. These measurements predicted electrical anomalies for a range of rock compositions which agree very well with the MT observations in the Himalaya (e.g., Unsworth et al. 2005). However, the viscosity values predicted for the inferred partial melt percentages (25–100 %) are orders of magnitude lower than the ones predicted by an earlier study by Rippe and Unsworth (2010), as discussed in more detail below.

3 Electrical Conductivity from MT Studies: What Do Crustal Anomalies Represent?

3.1 Physical Cause of Conductivity Anomalies in the Crust

Electrical conductivity anomalies in the crust are caused by interconnected fluids (including melt), graphite (interconnected), clay minerals, iron oxides and metallic sulphides.

Electrical conduction in most rocks is primarily electrolytic (ionic) caused by fluids in the pore space since most mineral grains and clay minerals are insulators or semiconductors. Exceptions are metallic sulphides, graphite and metals where conduction is electronic. The conductivity of most rocks therefore is dependent on the conductivity of the pore fluid and the pore space.

Near-surface conductive anomalies can be caused by fluids contained in the pore space of sediments producing the large conductors associated with sedimentary basins (e.g., Schäfer et al. 2011). The presence of clay minerals in the pore space can enhance the conductivity of sediment further. In a geothermal setting, this leads to the characteristic high conductive "clay cap" of high-temperature geothermal systems. Small amounts of clay which form during low-temperature alteration can dramatically increase the conductivity of resistive ignimbrites and other volcaniclastic material (Stanley et al. 1990; Bibby et al. 2005). An important transition occurring within conductive clay minerals is the dehydration from smectite to illite which takes place at ca. 65–150 °C and is marked by an increase in resistivity from <10 to 10–60 Ωm (e.g., Pellerin et al. 1996). In a subduction setting, this transition has a significant control on slip behaviour in sediments and has been associated with the onset of seismogenic slip along faults (Hyndman and Wang 1993).

Interconnected fluids lead to enhanced conductivity and occur in high-porosity or fractured rock (e.g., the damage zone around major faults). Excess fluid pressure and/or connectivity can also be produced by dehydration reactions (Wannamaker et al. 2002, 2009; Becken et al. 2008). Fluids enhance the generation of melting with increasing temperature; partial melts form in the crust in active tectonic areas such as subduction zones (e.g., Brasse and Eydam 2008; Heise et al. 2010), volcanic belts (e.g., Hill et al. 2009) or continental collision zones (Unsworth 2010) and can lead to considerable enhancement in electrical conductivity.

Conductivity anomalies in tectonically stable lithosphere were recently reviewed by Selway (2013). In the crust, these are thought to be mainly due to graphite around grain boundaries which can lower resistivity by several orders of magnitude (Duba and Shankland 1982). Examples of such crustal conductivity anomalies caused by carbon are described in, e.g., Jones et al. (2003); Heinson et al. (2006) and Pous et al. (2004). Carbon may also reduce shear strength in faults (Upton and Craw 2008); it can account for high conductivity in otherwise anhydrous crust and has been proposed as an alternative mechanism for crustal weakening in areas where the temperature is not sufficient for partial melting (Glover and Ádám 2008).

It is important to note, as mentioned in the Introduction, that from the conductivity model alone we cannot distinguish the physical cause of crustal electrical anomalies. Knowledge about the geodynamic setting (e.g., geological history, temperature) and laboratory measurements are important to establish a meaningful interpretation of the conductivity model. To use the results from conductivity models to interpret crustal deformation, the conductivity (or conductance) has to be transformed into parameters used in geodynamic modelling, e.g. viscosity. A two-step process is often necessary, e.g., (1) relating conductivity to melt percentage, fluid, clay or graphite content, and (2) relating the inferred melt/fluid/mineral content to physical parameters used in modelling such as viscosity, density or effective normal stress.

In summary, conductive anomalies in the crust are thought to be caused by fluids and melts; iron oxides and metallic sulphides; clay minerals; and/or graphite.

3.2 Melts

There are many examples in the literature where conductive anomalies have been quantitatively interpreted in terms of partial melt (e.g., Pous et al. 1995; Brasse et al. 2002; Heise et al. 2007; Didana et al. 2014). The melt (or fluid) fraction can be directly calculated from the bulk resistivity using mixing laws (assuming the melt conductivity is known). A number of mixing laws (e.g., Archie 1942; Hashin and Shtrikman 1962; Waff 1974; Glover et al. 2000) relate the bulk resistivity of the rock to the fluid content (porosity) and the conductivity of the fluid phase (for an overview see Glover 2010). However, these laws assume known melt conductivity and therefore only provide bounds for the melt percentage. To constrain the conductivity of the fluid phase, or to test results for specific temperature, pressure conditions and melt compositions, laboratory measurements are necessary.

Measurements of the conductivity of partially molten (crustal) rocks have been taken for different melt compositions and at temperature/pressure conditions yielding a relation between temperature and bulk resistivity. These measurements include hydrous and dry silicic melts (Waff and Weill 1975; Gaillard 2004), dacitic melts (Laumonier et al. 2014), thephrite to phonolite melt compositions (Pommier et al. 2008; Poe et al. 2008) and basaltic rocks (Tyburczy and Waff 1983; Gaillard and Marziano 2005). As an example, Schilling and Partzsch (2001) and Roberts and Tyburczy (1999) observed a steep increase in conductivity, using dry granulite samples, at the onset of partial melting at temperatures >1030 °C. A recent laboratory study by Hashim et al. (2013) was conducted to constrain the melt percentages in the Himalaya at lower crustal depth. Here, measurements of the conductivity of metapelites under relevant pressure (300 MPa) and varying temperature conditions were taken. Melt percentage and bulk resistivity of the sample were obtained at different pressure–temperature conditions. At 850 °C, a melt percentage of 23 % is reached. However, the authors state that this melt percentage is expected to be reached quickly above muscovite breakdown temperature at $T > 650$ °C and that slow melt kinetics are responsible for the higher temperatures observed. This was also confirmed by measurements during cooling cycles where the melt fraction stayed high until 500 °C.

An application "*SIGMELTS*" to calculate the conductivity of melts has been developed by Pommier and LeTrong (2011). *SIGMELTS* calculates the conductivity of a two-phase material from existing geometric models at defined conditions at crustal and upper mantle depth. A model to relate viscosity to conductivity of silicate melts has been derived by Pommier et al. (2013) by using a database of laboratory measurements of conductivity and viscosity (Giordano et al. 2008). However, they point out that viscosity is much more sensitive to melt composition (e.g., large difference for basaltic and dry rhyolitic melt) and water content than electrical conductivity, and therefore, melt composition has to be well known.

To complete the link to rheology and modelling, the viscosity of the partially molten rock has to be determined for different melt percentages. The melt fraction is a key parameter determining the strength and effective viscosity of the rock (e.g., Arzi 1978; Rosenberg and Handy 2005). Laboratory measurements have shown that the largest viscosity decrease takes place at melt percentages of 1–5 %, while a second less significant drop in viscosity takes place at 25–30 % (Rosenberg et al. 2007; Jamieson et al. 2011) (Fig. 1a). The cause of the strength reduction at melt percentages of <10 % is the increase in intergranular connectivity at the onset of melting. The decrease in strength at <10 % magma is called the first rheological transition or *melt connectivity threshold* (MCT).

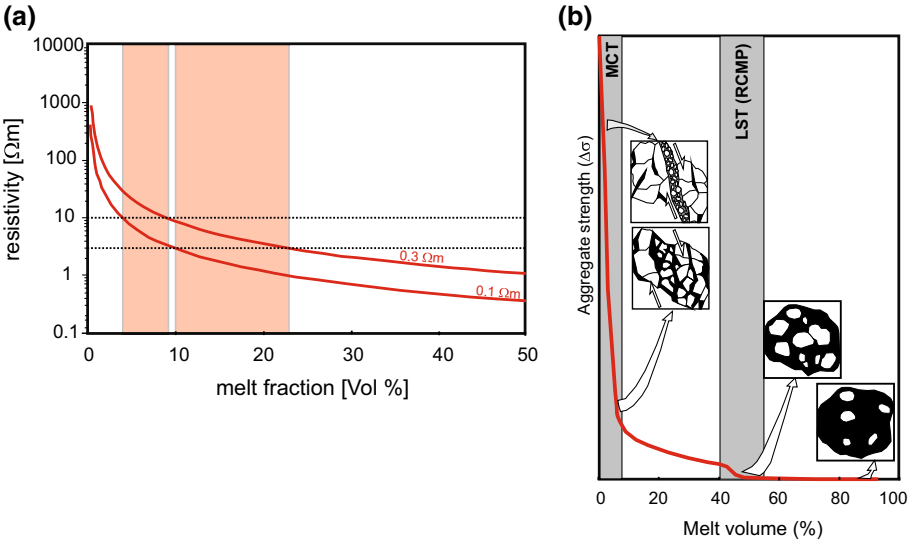

Fig. 1 **a** Bulk resistivity as a function of melt fraction obtained from Archie's law for melt resistivities of 0.1 and 0.3 Ωm. The *red shaded areas* show melt required to explain conductivity of the northern Lhasa block (4–9 %) and the southern Lhasa block (10–23 %) in the Himalaya (redrawn from Rippe and Unsworth 2010). **b** Aggregate strength versus melt fraction for partially molten granite. The decrease in strength at <10 % magma is the first rheological transition or melt connectivity threshold (MCT), caused by the increase in intergranular connectivity at the onset of melting. At 10–20 % melt, the rock consists of a solid matrix with a network of interconnected melt channels. At 40–60 % melt, the solid rock framework breaks down, and this is called the rheologically critical melt percentage (RCMP) or solid-to-liquid transition (redrawn from Rosenberg and Handy 2005)

Above 10 % melt, the rock consists of a solid matrix with a network of interconnected melt channels. At melt fractions of 40–60 %, the solid rock framework breaks down, and this is the so-called *rheologically critical melt percentage* (RCMP) or *solid-to-liquid transition* (SLT). For characterizing crustal flow, the most important rheological transition is the MCT (Fig. 1b; Rosenberg and Handy 2005). Such melt weakening can have a dramatic effect on the dynamics of rifts and other tectonic settings (e.g., Buck and Lavier 2001; Beaumont et al. 2006; Schmeling 2010; Ellis et al. 2011).

For non-melt-related anomalies, the relationship to physical parameters in models is more qualitative. Measurements on carbon-bearing rock samples have been taken by Glover and Ádám (2008), showing that progressive shearing weakens the rock and results in higher conductivity. This suggests that ductile shear zones at depth may be associated with MT anomalies, providing a possible way to link the MT observations to geodynamic model predictions of shear localization.

The transition in mineral phases with increasing depth can be accompanied by conductivity changes. This is well known in geothermal exploration where clay mineral transitions can be linked to conductivity changes and temperature, e.g., the transition from smectite to illite (Ussher et al. 2000; Björnsson et al. 1986). In subduction settings, these transitions may be able to be used to constrain predictions from thermo-mechanical geodynamic models for temperature, pressure and rock composition at depth (e.g., Saffer et al. 2012; Heise et al. 2012). It is therefore important to quantify conductivity anomalies

caused by metamorphic phase transitions and/or presence of fluids as they may affect the strength of ductile and brittle rocks.

3.3 Interpretation of Crustal MT Anomalies Using Geodynamic Models

3.3.1 Partial Melt, Viscosity, Crustal Flow: The India–Asia Collision

In continental collision settings, the crust can be thick and hot enough to start melting, which lowers the viscosity of the crust. The India–Asia continent–continent collision zone has been extensively studied by magnetotelluric surveys, many of them as part of the International Deep Profiling of Tibet and Himalaya (INDEPTH) project (Chen et al. 1996; Unsworth et al. 2004, 2005; Spratt et al. 2005; Ye et al. 2007; Arora et al. 2007). For a review of all MT work that has been carried out in the Himalaya and Tibetan Plateau until 2010, see Unsworth (2010). The most recent studies of the eastern Himalayan have been carried out by Zhao et al. (2012) and Wang et al. (2013). All of these studies found a mid-crustal (15–20 km depth) conductive layer associated with the Tibetan plateau (e.g., Fig. 2). This conductor has been interpreted as partial melt, since in the Himalaya temperatures >700° are reached within the crust (Klemperer 2006), exceeding the temperature where dehydration melting of muscovite starts.

Flow of low-viscosity material owing to the presence of partial melt has been used to explain the topography and uplift history of the Himalayas (e.g., Beaumont et al. 2006). A simple model predicts channel flow of a viscous fluid between two rigid plates due to a lateral pressure gradient. In the Himalaya, channel flow has been proposed to occur in a layer of partially molten migmatite decoupled from the upper and lower crust, helping to explain inverted metamorphic sequences observed there (Jamieson et al. 2011).

Interpretation of the mid-crustal conductive layer as partial melt or aqueous fluid or a combination of both is not unambiguously possible from the MT data alone (see extensive discussion in Li et al. 2003). Motivated by the geodynamic model of Beaumont et al. (2001) predicting a zone of partial melting, the conductive anomaly was assumed to be predominantly partial melt in some MT studies. Unsworth et al. (2005) calculated the melt

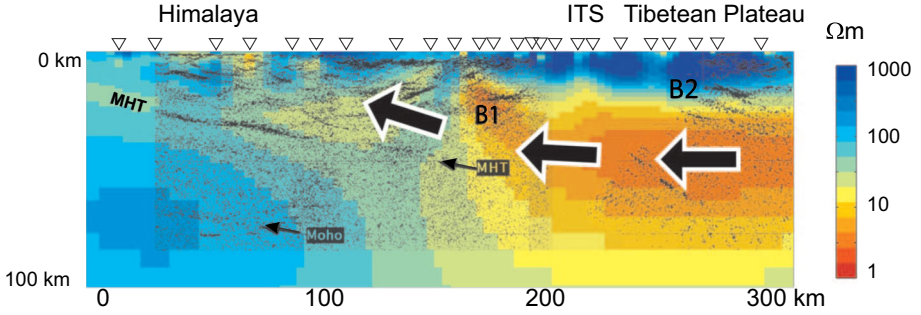

Fig. 2 Crust below the Himalaya and southern Tibetan plateau (after Unsworth et al. 2005 and Jamieson et al. 2011). *Black lines* show seismic reflection data from the INDEPTH profile (Nelson et al. 1996). *MHT* Main Himalayan Thrust, interpreted as the upper surface of the underthrust Indian plate. MT model by Unsworth et al. (2005). The low resistivity indicates the presence of a fluid phase (e.g., partial melt); reflector B2 is interpreted to represent the top of a fluid (melt)-bearing region. *Arrows* show possible flow direction leading to exposure of mid-crustal melt zones in the High Himalaya. *ITS* Indus–Tsangpo suture (defines the plate boundary at the surface)

fraction from the bulk resistivity by using the model of Schilling et al. (1997) and conclude the viscosity drop due to partial melt might enable crustal flow.

Recently, Rippe and Unsworth (2010) attempt to quantify this and establish a relationship between conductance, flow velocity and effective viscosity, thus giving an example how rheological parameters can be calculated from a MT model. In Tibet, the flow is regarded to be mainly driven by the pressure gradient due to topography, i.e. Poiseuille flow (Clark and Royden 2000; Beaumont et al. 2001, 2004). The mean velocity of the Poiseuille flow and the effective viscosity depend on the channel thickness h and can be expressed in terms of conductance of the conductive "channel" determined from the MT. Melt fraction was calculated using Archie's law. Most rocks deform as non-Newtonian fluids (Carter and Tsenn 1987) which means their viscosity is dependent on the strain rate and thus shear stress and strain rate are related by a material constant A_{eff} (in the case of Newtonian fluids A_{eff} is the dynamic viscosity). The rheological material constant A_{eff} and bulk electrical resistivity (ρ) both decrease with increasing melt fraction, and therefore, a direct relationship between these two parameters can be determined.

For a varying conductance, two cases are possible: (1) the bulk resistivity stays constant and the thickness of the conductive channel changes, so that relations between flow velocity/effective viscosity and conductance are linear; or (2) the thickness stays constant and the bulk resistivity changes. Since bulk resistivity is needed to calculate the material constant A_{eff}, the relation between mean velocity/effective viscosity and conductance is then more complex. Flow velocity and effective viscosity obtained from magnetotelluric models for different regions in the Himalaya have then been compared to the viscosity values used in geodynamic models (e.g., Beaumont et al. 2001; Clark and Royden 2000; Copley and McKenzie 2007).

However, despite such a thorough analysis, a number of assumptions were required to make this calculation, including the assumed felsic composition of the crust, the thickness of the layer and the temperature and pressure of the laboratory measurements. As Rippe and Unsworth (2010) point out, accuracy of the temperature estimate is probably the most critical point in the calculation, since temperature has a large influence on melting and thus viscosity. A more recent laboratory study by Hashim et al. (2013) suggests much higher melt percentages (>25 %) and corresponding lower viscosities than predicted in the previous studies; the authors suggests a recalibration of the MT models with their new values.

For completeness, we will mention a contrary explanation for the uplift of the Himalayan orogen given by Harris (2007). This paper offers a critical analysis of the channel flow models discussed above, claiming that there is no evidence for the persistence of crustal flow since the mid-Miocene. They support alternative models for Himalayan uplift and deformation, with formation of an orogenic wedge and thickening by underplating at the brittle–ductile transition (Toussaint et al. 2004; Bollinger et al. 2006). Harris (2007) also states that some magnetotelluric anomalies in the central Himalaya have been interpreted as crustal fluids from dehydration reactions (Lemmonier et al. 1999).

3.3.2 *Fluid Interconnectivity, Grain-Size Reduction and Shear: The Alpine Fault and Marlborough Fault Systems of New Zealand*

In the South Island of New Zealand, the Alpine Fault is the primary structure that accommodates oblique collision between Pacific and Australian continental crust (Norris et al. 1990). A broad, "U-shaped" zone of high electrical conductivity with a maximum depth of ca. 25 km is imaged in the ductile crust, extending near vertically downward below the Alpine Fault to a sub-horizontal zone below (Wannamaker et al. 2002; Jiracek

et al. 2007). Based on predictions from numerical modelling (Koons et al. 1998; Upton et al. 2000), the high-conductivity anomaly has been interpreted to be a zone of interconnected fluids along grain boundaries in the quartzo-feldspathic rocks. The fluids may arise either from prograde and strain-induced metamorphism in the underlying zone of crustal thickening, or from strain-induced metamorphism in the high-strain-rate mylonite zone beneath the Alpine Fault (Koons et al. 1998; Wannamaker et al. 2002).

At the northern end of the Alpine Fault, plate motion is taken up along multiple strike-slip crustal faults (the Marlborough Fault System) as result of the transition of subduction to oblique collision. Here, anomalous regions of low-Q (high attenuation) are imaged seismically directly beneath some of the Marlborough Faults, similar to anomalous conductive regions imaged in the MT profile (Wannamaker et al. 2009). The MT profile shows two distinct low-resistivity zones (<50 Ωm) in the ductile lower crust, which Wannamaker et al. (2009) interpret as broad, fluid-rich shear zones associated with the major strike-slip faults above (see also Ogawa and Honkura 2004).

Eberhart-Phillips et al. (2014) compared the Q and resistivity anomalies for the Marlborough Fault System to a numerical model of strain localization beneath brittle strike-slip faults (Fig. 3a–d). The numerical model showed how faults act to localize strain below them in the ductile crust, with elevated strain rates and stresses. These are predicted to cause grain-size reduction (formation of mylonite zones) over time. In ductile crust, Q is influenced by temperature, grain size, water and mineral content. Eberhart-Phillips et al. (2014) relate the Q anomaly to grain-size reduction associated with elevated strain rates in a mylonite zone. Reduced grain size will also lead to a decrease in electrical resistivity, as has been observed for forsterite by ten Grotenhuis et al. (2004) who also created a geometric model that matches the experimental observations. This geometric model has been applied to mylonite shear zones and shows that conductivity contrast between fine-grained shear zones and less-deformed regions in the lithosphere can be 1.5–2 orders of magnitude.

4 Electrical Conductivity from MT Studies: What Do Mantle Anomalies Represent?

4.1 What Causes Conductivity Anomalies in the Mantle

Mantle conductivity is influenced by temperature and composition and by the amount of fluid phases present, either as melt, hydrous water in pores or H^+ content in anhydrous minerals. Likewise, the rheology of the mantle is constrained by these parameters (e.g., Bürgmann and Dresen 2008). Conductivity anomalies in the mantle have been interpreted as either melt, or water dissolved in olivine; however, there is a debate about the effect of water on the conductivity of olivine (see below). Gaillard et al. (2008) also point at the possibility of carbonatite melts in the mantle, which are orders of magnitude more conductive than silicate melts and hydrous olivine, and could account for some of the high conductivities observed in MT data (e.g., Evans et al. 2005).

In the upper mantle, conductivity anomalies have been found associated with subduction zones and spreading centres and have been interpreted as partial melt and upwelling asthenosphere (e.g., Naif et al. 2013; Key et al. 2013; Rippe et al. 2013). The long-period 3-D MT model obtained from array data in the north-western United States includes interpretations for upper mantle conductivity heterogeneities in a variety of different tectonic settings (Meqbel et al. 2014).

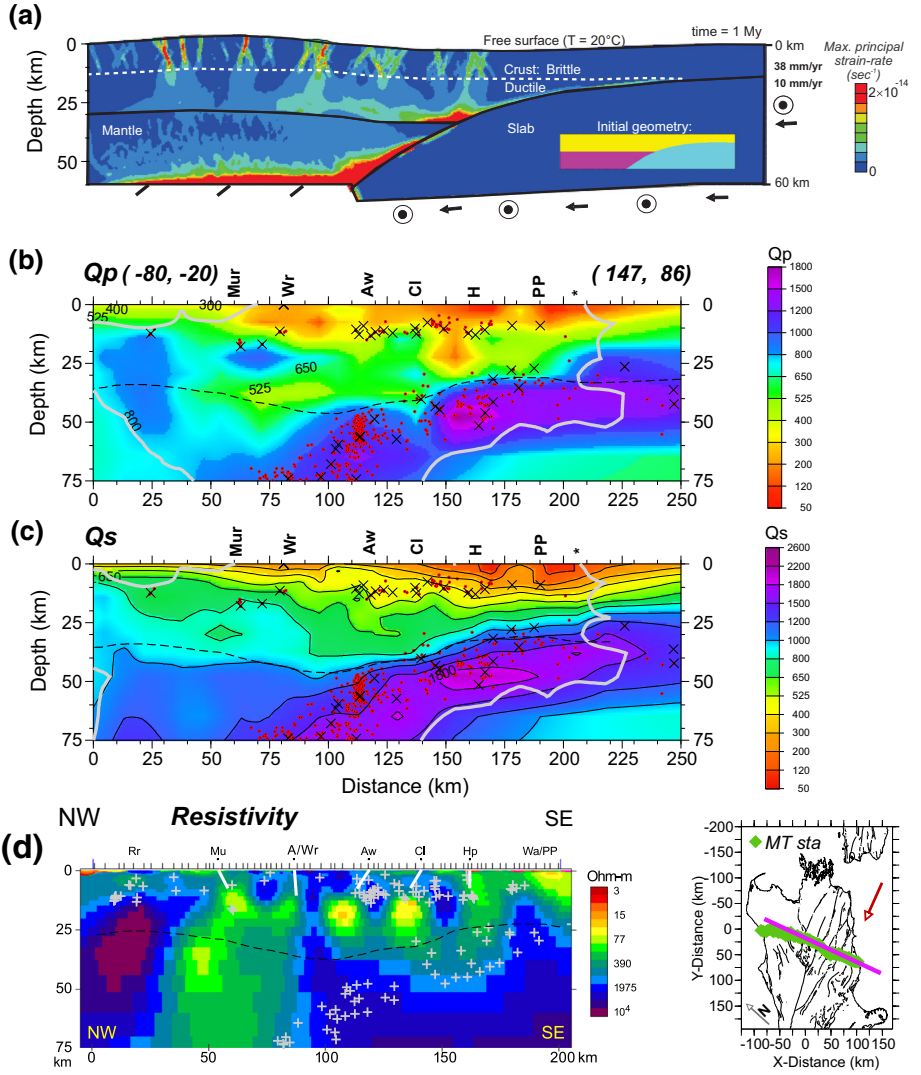

Fig. 3 Comparison of strain rate from a geodynamic model (**a**), seismic quality factor (the inverse of attenuation) for *P*-waves (**b**) and *S*-waves (**c**), and resistivity inversion from MT (**d**). **a** Velocity boundary conditions by *arrows* (normal convergence) and *dots* with *circle* (dextral displacement). Colour contours of maximum principal strain rate are shown after 1 Myr of oblique compression, showing localized deformation (*red*) in 4–6 main semi-vertical fault strands. *White dashed line* indicates brittle–ductile transition in crust. **b** *Qp* and **c** *Qs* cross sections across the faults, along magenta line in inset map, with hypocentres for 2001–2012 seismicity (*red circles*) and inversion earthquakes (*pluses*). *Black dashed lines* show the $Vp = 7.5$ km s^{-1} contour, as a pseudo-Moho. *Grey lines* for low resolution indicate a contour of data quality; areas outside of the region enclosed by this contour are not well constrained in the seismic inversion (see Eberhart-Phillips et al. 2014 for details). *Asterisk*, coast; faults, Mur, Murchison; Wr, Wairau; Aw, Awatere; Cl, Clarence; H, Hope; PP, Porters Pass. **d** Cross section of resistivity determined by Wannamaker et al. (2009), including their interpreted faults, from magnetotelluric data along the profile indicated by green diamonds on the *inset map* (after Eberhart-Phillips et al. 2014)

Upwelling and mantle flow define large-scale global geodynamics. Mantle viscosity is an important parameter in mantle flow models, and in these large-scale models, it is generally linked to fluid content. Since dissolved water content in mantle minerals can lower the electrical conductivity by up to three orders of magnitude (Karato 2011), where melting is unlikely owing to great pressures, conductivity can be used to infer water content in the mantle and thus MT provides a tool to give constraints on mantle rheology.

In summary, conductive anomalies in the mantle represent either: partial melt; hydrous water in pores; and/or H+ content in anhydrous minerals.

4.2 Constraints on Fluid and Melt Content from Laboratory Studies of Conductivity

The conductivity of dry and anhydrous olivine has been widely studied by different laboratories. Major contributions are found in Poe et al. (2010), Yoshino et al. (2009), Karato (2011) and Wang et al. (2006). However, Yoshino et al. (2009) and Poe et al. (2010) obtain significantly lower conductivities for the same water content as Wang et al. (2006) or Karato (2006), thus resulting in different conductivity depth profiles for the mantle. The recent review paper by Pommier (2013) gives an overview of results of the main laboratory studies for the conductivity of mantle minerals and also discusses the discrepancies, which may be caused by different water content in the "dry" olivine samples or different experimental design, though this issue remains contentious. A detailed description of the different formulations of the Arrhenius equation used to fit the data in the experiments is given by Rippe et al. (2013) and Jones (2014). The latter paper also points out that discrepancies in the laboratory results impede a non-ambiguous interpretation of conductivity anomalies in the mantle. Many MT mantle studies therefore use different datasets to put bounds on water content and melt fraction of the mantle (e.g., Rippe et al. 2013; Khan and Shankland 2012).

4.3 Interpretation of Mantle MT Anomalies Using Geodynamic Models

4.3.1 Mantle Upwelling and Flow: The East Pacific Rise

Mantle conductivity and mantle upwelling at the East Pacific Rise have been studied by long-period magnetotelluric measurements at the southern segment of the East Pacific Rise as part of the Mantle Electromagnetic and Tomography (MELT) project (Evans et al. 2005; Baba et al. 2006). More recent studies have been carried out on the northern East Pacific Rise (Key et al. 2013). In both studies, geodynamic modelling of the mantle flow and temperature reproduced a temperature velocity field which was compatible with the shape of the melt producing region (conductive anomaly) detected by the MT study. In these examples, geodynamic models were created for direct comparison with the resistivity model and reinforced the interpretation of MT study.

Evans et al. (1999) show that the conductivity anomaly below the southern East Pacific Rise is asymmetric, with a conductive mantle (80–150 km) containing fully interconnected (3 %) melt fraction west of the ridge, while the mantle east of the ridge is more resistive and is interpreted as being melt-depleted. The difference in spreading velocities between Nazca and Pacific Plates is suggested to be the cause for this asymmetry; however, the authors pointed out that geodynamic models of the mantle flow are needed to support this interpretation. These were implemented by Toomey et al. (2002), who showed that the asymmetric flow produced by the plate motion was not sufficient to reproduce the

anomalies east of the spreading centre (they compared predictions to observed higher electrical conductivity, greater seafloor subsidence, lower seismic velocities and greater shear wave splitting to the east). A combination of an asymmetric mantle flow field and a thin and hot asthenospheric channel was needed to explain the anomalies.

A broadband magnetotelluric survey was carried out across the northern East Pacific Rise by Key et al. (2013). This study revealed a more detailed picture of the upper mantle and mantle upwelling beneath the ridge, providing constraints on melting processes and the volatile content of the mantle. The MT models show a large, symmetric, highly conductive zone beneath the ridge, interpreted as a partial melt fraction of up to 10 % in the upwelling mantle. A deeper conductive anomaly interpreted as carbonate melts is displaced to the east. A 3-D mantle flow simulation was then carried out in order to find an explanation for the deeper asymmetry in the model. The 3-D flow modelling used a finite-element approach, taking into account the absolute plate motion as well as the transform faults north and south of the studied ridge segment. The vertical velocity field was used as a proxy indicator for where deep melt could be formed. The predicted vertical velocity cross section showed that, contrary to the case for the southern East Pacific Rise, the deep conductive melt body only requires passive flow (Fig. 4).

4.3.2 Mantle Flow and Anisotropy

Electrical anisotropy at lower crustal and upper mantle depths has been inferred from MT studies and been related to mantle flow (Simpson 2001; Bahr and Simpson 2002; Gatzemeier and Moorkamp 2005). One explanation for the anisotropy is the alignment of olivine crystals with respect to plate movement (lattice-preferred alignment). Since hydrogen diffusion in olivine crystals is strongly anisotropic (Kohlstedt and Mackwell 1998), the ionic conductivity of olivine mantle where the crystals are aligned should be electrically anisotropic. Experimental evidence for the alignment of olivine crystals due to dislocation creep of the upper mantle has been given by compression creep experiments on fine grain olivine (Miyazaki et al. 2013). Although seismic and electrical anisotropy have been related in several studies (e.g., Eaton et al. 2004; Ji et al. 1996), this comparison can be only made in simple cases (for a discussion, see Heise et al. 2006). In a recent paper, Simpson (2013) showed that electrical anisotropy generated by hydrogen diffusivity in aligned olivine at mantle depth has an anisotropy factor of <4.5. Therefore, in other cases where much stronger electrical anisotropy in the mantle has been inferred from magnetotelluric models (e.g., Bahr and Simpson 2002; Gatzemeier and Moorkamp 2005), the anisotropy needs to be explained by other mechanisms, or isotropic heterogeneities have to be considered to explain the data (e.g., Korja et al. 2002).

Caricchi et al. (2011) showed that anisotropy of electrical conductivity can be generated by interconnected melt channels in the spreading direction and low melt connectivity in the ridge parallel direction. The presence of oriented melt channels explains high anisotropic values as observed at the southern East Pacific Rise (Evans et al. 2005; Baba et al. 2006).

4.3.3 Can Global Resistivity Models be used to Constrain Mantle Viscosity in Convection Models in the Future?

Conductivity anomalies in the deep mantle and transition zone, where melt is suppressed by high pressures, are thought to reflect variations in water content. Water lowers viscosity and solidus of mantle minerals and seismic velocity, and its distribution therefore plays an important role in the dynamics of the mantle. The lateral variations in the

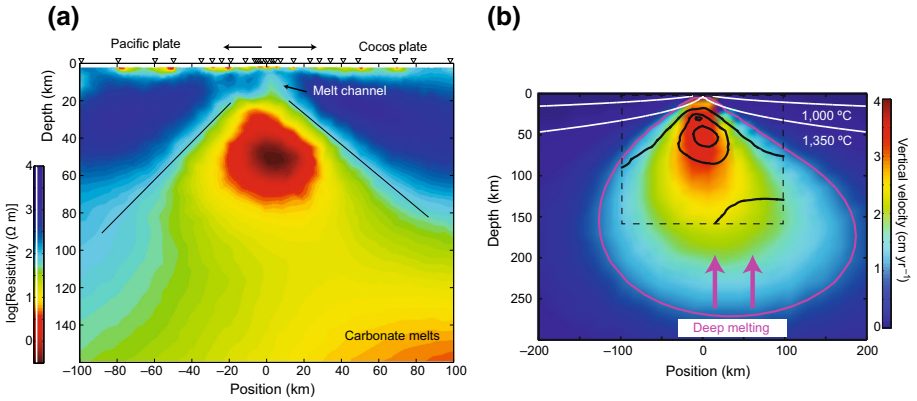

Fig. 4 **a** MT inversion model showing the conductive anomaly interpreted as upwelling of partially molten mantle beneath the northern East Pacific Rise. **b** *Colour* shows the flow model, showing predicted vertical velocity anomaly due to plate movement. The *magenta line* shows the region where the vertical flow is >1 cm/year. *Black lines* delineate 0.1, 1 and 10 Ωm resistivity contours from the magnetotelluric inversion model (**a**). *White lines* show isotherms for a half space cooling model (from Key et al. 2013)

electrical conductivity structure of the deeper mantle (up to depth of 1200 km) have been explored by studies of very-long-period measurements using observations at geomagnetic observatories worldwide (e.g., Kelbert et al. 2009a; Kuvshinov et al. 2005; Khan et al. 2010).

A method to include laboratory measurements has been developed by Khan and Shankland (2012). A conductivity profile of the mantle is calculated at four locations from geomagnetic observatories and combined with laboratory-based conductivity models to constrain the thermo-chemical state of the mantle. This approach takes into account known geophysical and petrological discontinuities that could not be resolved with the inversion of electromagnetic data. However, as the authors note, this method depends on laboratory measurements; they stress the importance of an improved conductivity database for the mantle. The use of the two contrasting databases Yoshino et al. (2009) and Karato (2006) resulted in a melt layer and a dry mantle transition zone, respectively.

A recent review by Kuvshinov (2011) summarizes and compares the global electromagnetic models, but there is still a discrepancy between 3-D conductivity distributions obtained by different groups (e.g., Semenov and Kuvshinov 2012; Kelbert et al. 2009a, b) due to different modelling approaches and data sets, thus making comparison and use for geodynamic modelling difficult. Although Kelbert et al. (2009a) and other authors stress the importance of the global resistivity models to constrain water content in the mantle and thus dynamics, at the present time no study directly relates or uses the results for geodynamic models of mantle convection. Better resolution of global conductivity models via improved data coverage from satellites and observatories would give the potential to incorporate constraints from conductivity models into global convection models in the future. Global mantle convection models already include lateral viscosity variations inferred from seismic tomography, which fit the observed plate motions more realistically than models with simpler radial viscosity profiles (e.g. Becker 2006) and also fit mantle strain estimated from lattice-preferred orientations in olivine aggregates from seismic anisotropy (Tommasi et al. 2000; Kaminski et al. 2004). Lateral variations of mantle

viscosity could be also constrained by global conductivity models. Although this has not yet been tested, we believe there is great potential in combining global conductivity and convection models.

5 Integration of Geodynamic Models and EM: The Way Forward

As discussed above, the interpretation of crustal resistivity anomalies is non-unique and no direct method exists for linking resistivity to rheological parameters and/or fluid. For these reasons, not many studies have input MT resistivity results directly into numerical models of geodynamics. Nevertheless, some studies have taken a small step in this direction.

5.1 Applications in Economic Geology

An MT model was successfully used as input for geodynamic modelling for exploration in China (Liu et al. 2011). In the Anqing ore field, the known ore reserves are located in the contact zone between a diorite intrusion and the host rocks consisting of Lower–Middle Triassic carbonates. Evaluating the effect of the distinct, uneven distribution of the ore bodies along the contact zone on mineralization required interpretation by a geodynamic model describing the mineralization processes associated with the intrusion; the ore mineralization formed during the cooling of the intrusion.

A conductivity survey of the Anqing ore field was conducted using a direct source magnetotelluric instrument (Strategem EH4). Two hundred-metre-spaced profiles over the mining area were measured and 2-D modelling carried out for each profile. The main feature of the resistivity model is the contact between high resistive carbonate sediment and the moderate resistive diorite. The geometry of the contact was used to construct the initial model for the geodynamic modelling. The geodynamic models used the two-dimensional finite-difference code FLAC (Itasca 2002) to simulate deformation, heat transfer and fluid flow during the syn-deformation cooling of ore-related intrusion. Results show that there is a close correlation between the known ore bodies and dilation zones in the model, which are mainly along the contact (Fig. 5). An exploration target in a deep dilation zone was identified from the model, and a new ore body was discovered, thus demonstrating a successful and useful integration between geodynamic modelling and electromagnetic constraints.

5.2 Using Temperature and Melt Fraction from Geodynamic Modelling to Constrain a 3-D MT Forward Model of the Icelandic Plume

Numerical models of the Icelandic plume–ridge system have been carried out to model the present-day dynamics of the plume and the melt generation in the upper mantle. The models were aimed at reproducing the observed thickness of the Icelandic crust. Parameters varied were temperature anomalies and retained melt fraction (Ruedas et al. 2004). The resulting melt and temperature fields were then used to calculate seismic velocities and 3-D conductivity models. The melt percentage in the plume head of the conductivity models was varied—within the bounds given by the geodynamic models—and compared to "ridge only" models (Kreutzmann et al. 2004). The synthetic MT data calculated from these conductivity models were then analysed to separate the effects of ridge and plume. A

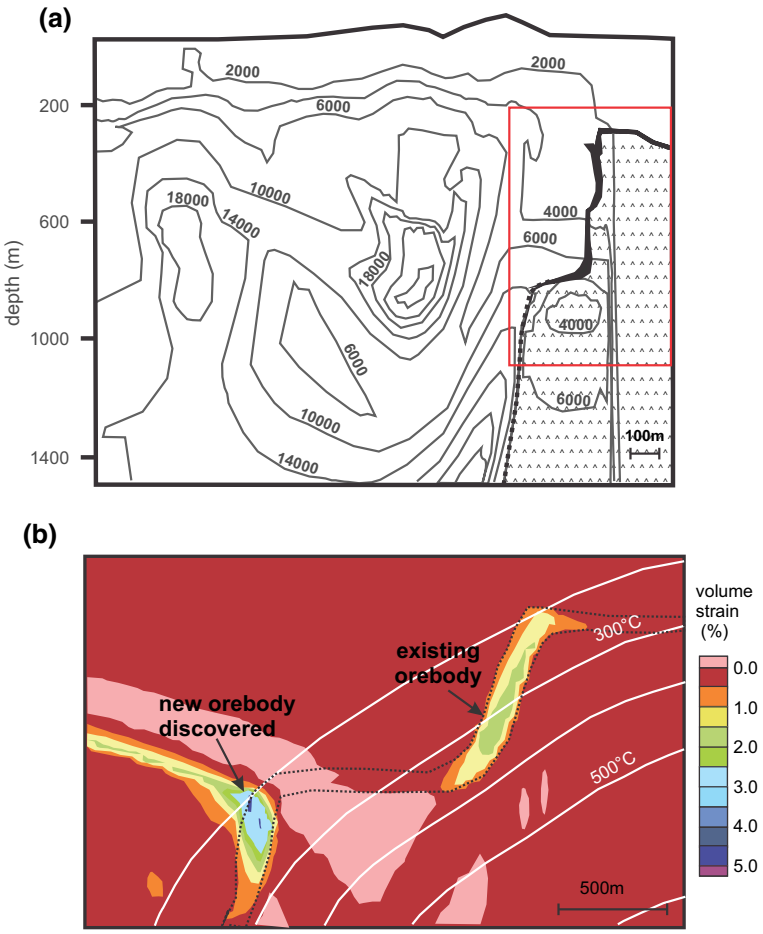

Fig. 5 (Redrawn from Liu et al. 2011) **a** *Grey contour lines* show the resistivities from the controlled source MT profile, the *black line shows* the contact between marble and intrusion where it is known from drilling, the *dashed line* shows the boundary interpreted from the resistivity model (note the vertical exaggeration), and *red line* shows approximate area of the geodynamic model shown in (**b**). **b** Deformation and temperature predicted by the geodynamic model. Isotherms and total volumetric strain contours are shown after 9200 years of deformation, and the dashed *black line* is the contact zone deduced from the MT model. For the pore fluid flow field, see original figure in Liu et al. (2011)

minimum melt percentage of 3 % in the plume head was established as bound for detecting the plume in the MT data; however, comparisons between these synthetic models and real data could not be done due to the lack of very-long-period MT data.

5.3 Using MT to Quantitatively Constrain Crustal Models of the Taupo Volcanic Zone, New Zealand

Ellis et al. (2014) illustrate how a "partial coupling" between MT inversion results and geodynamic modelling in 3-D might work by taking MT resistivity anomalies from a 3-D

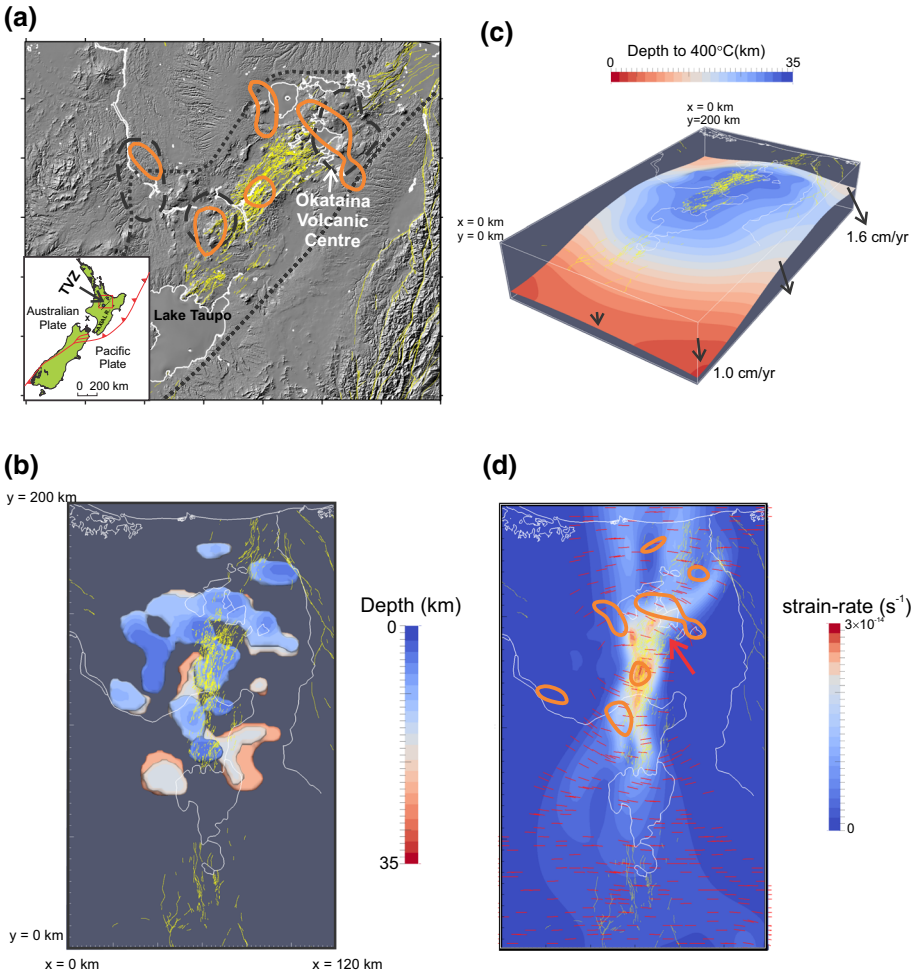

Fig. 6 (3-D model). **a** The Taupo Volcanic Zone (TVZ) is an intra-arc rift associated with westward subduction of the Pacific plate beneath the North Island of New Zealand (*inset*). Active fault traces are shown in yellow (Litchfield et al. 2014), and *dotted lines* indicates extent of TVZ (envelope of volcanic activity in last 2 My) from Wilson et al. (1995). *Dashed black lines* show outlines of volcanic centres. *Orange lines* outline the 5 Ωm contour at 13 km depth from MT inversions by Heise et al. (2010), and *white lines* show coast, lakes and rivers. **b** Contoured volumes are regions with resistivity <10 Ωm colour coded by depth. *Yellow* are active faults. **c** Set-up of 3-D numerical model. Surface, contoured by depth in km, is depth to 400 °C isotherm derived from steady-state thermal solution with total magma body heat output ca. 4GW. *Black arrows* show applied boundary condition assuming a pole of rotation from Nicol and Wallace (2007). **d** Colour contours show surface strain rate (second invariant) indicating a high-strain-rate zone in red at the surface. *Red lines* are direction of maximum brittle stretch (normal faults should form perpendicular to these lines). *Red arrow* indicates change in strain-rate trend predicted from geodynamic model and resulting from distribution of partial melt at depth inferred from MT. This change in trend mirrors the change in active fault strike (*yellow lines*)

crustal inversion of the Taupo Volcanic Zone (New Zealand) (Heise et al. 2010; Fig. 6a) as an input parameter to a 3-D thermo-mechanical model (Ellis et al. 2011). In conducting this test, the following assumptions were made:

- Resistivity below 10 Ωm at depths greater than 6 km represents partial melt (Heise et al. 2010). Low resistivities at shallow depths are assumed to be regions with altered clays and sediments associated with hydrothermal and basin deposits and are not used to constrain the numerical model (Fig. 6b).
- The low-resistivity mid-crustal regions are defined as crustal material with a partial melt content using an approximation of the curve shown in Fig. 1a from Rippe and Unsworth (2010) and based on Archie's law. This is clearly a simplification, since there is a trade-off between the size of the anomaly and how much partial melt it represents (see discussions above).
- The zones of partial melt have a lower viscosity and density than surrounding crustal regions (Ellis et al. (2011), following Rosenberg et al. (2007)). This relationship is used to reduce the base strength for each location, which is computed assuming a quartzo-feldspathic crustal composition, with brittle Byerlee's law giving way to temperature- and strain-rate-sensitive nonlinear viscous creep with increasing depth. For a partial melt of 20 %, viscosity drops by a factor of about 10^4 and density from 2800 kgm^{-3} (no melt) to 2500 kgm^{-3}.
- The region of active rifting in the TVZ has anomalously high heat flow and a seismogenic depth of less than 7 km (Bibby et al. 1995; Bryan et al. 1999). Total heat output in the central TVZ is estimated at $\sim$4 GW (Bibby et al. 1995). For the simple test in Ellis et al. (2014), the effects of elevated heat flow from cooling magma bodies at depth were represented by imposing a high heat production in the partial melt bodies defined from MT. The heat production was adjusted to give a shallow brittle–ductile transition depth for the central TVZ matching seismological observations (Bryan et al. 1999). This was used, along with a basal heat-flux of 30 mWm^{-2}, to compute a steady-state thermal field throughout the region (Fig. 6c).

Figure 6d shows the predicted zone of high strain rate for the numerical model in Ellis et al. (2014). Interestingly, a zone of high strain rates was predicted that mirrors the mapped locations and trends of active faults in the central TVZ (Villamor and Berryman 2006). The concentration of shallow partial melt around the Okataina Volcanic Centre (Fig. 6a) and the change in the axis of partial melt along strike are responsible for the jog in fault trend (red arrow, Fig. 6d). In comparison, models without the low-strength, high-heat-flow partial melt bodies derived from MT cannot match rift dynamics and the pattern of active faulting seen in the TVZ; instead, a broad region of extension occurs over more than 80 km across the rift.

The agreement between the locus of active faulting and the change in fault trend just south west of the volcanic centre of Okataina suggests that the location of partial melt in the TVZ rift significantly affects rift dynamics and faulting. However, several issues need to be considered further when applying MT results to geodynamic models in this way. The first is the trade-off between size and magnitude of the low-resistivity bodies. A sensitivity study to see how this affects dynamics in the geodynamic model has not been undertaken. Near-surface conductive features may also be influencing the MT inversion at depth. Finally, it was not possible to simply take the inversion results from MT straight into the geodynamic model. Low-resistivity bodies shallower than 6 km were discounted on geological grounds, because most represent clay-rich sediment deposits, but there is some evidence for shallower magma bodies in the TVZ (e.g., Bertrand et al. 2012). Even so, some of the bodies represented as partial melt in Fig. 6b are well away from the rift axis and may be caused by some other physical process.

5.4 Using Results from a Geodynamic Model of Melt in a Rift to Predict MT Resistivity

In an earlier paper, Kissling and Ellis (2011) used a thermo-mechanical code to model the evolution and deformation of a continental rift (e.g., the Taupo Volcanic Zone) over millions of years. This model predicts the change in crustal properties and the evolution in the brittle–ductile transition and the formation of partial melt (Fig. 7a, b, c). Their model set-up was a 30-km-thick crustal layer above the mantle. Elevated heat flow was applied over a narrow zone at the base of the model and after 2 My extension was applied to the sides as shown in Fig. 7a. After 8 Ma, deformation moved from the rift flanks to the central faults and a thin (∼1 km thick) layer of partial melt developed at the base of the crust.

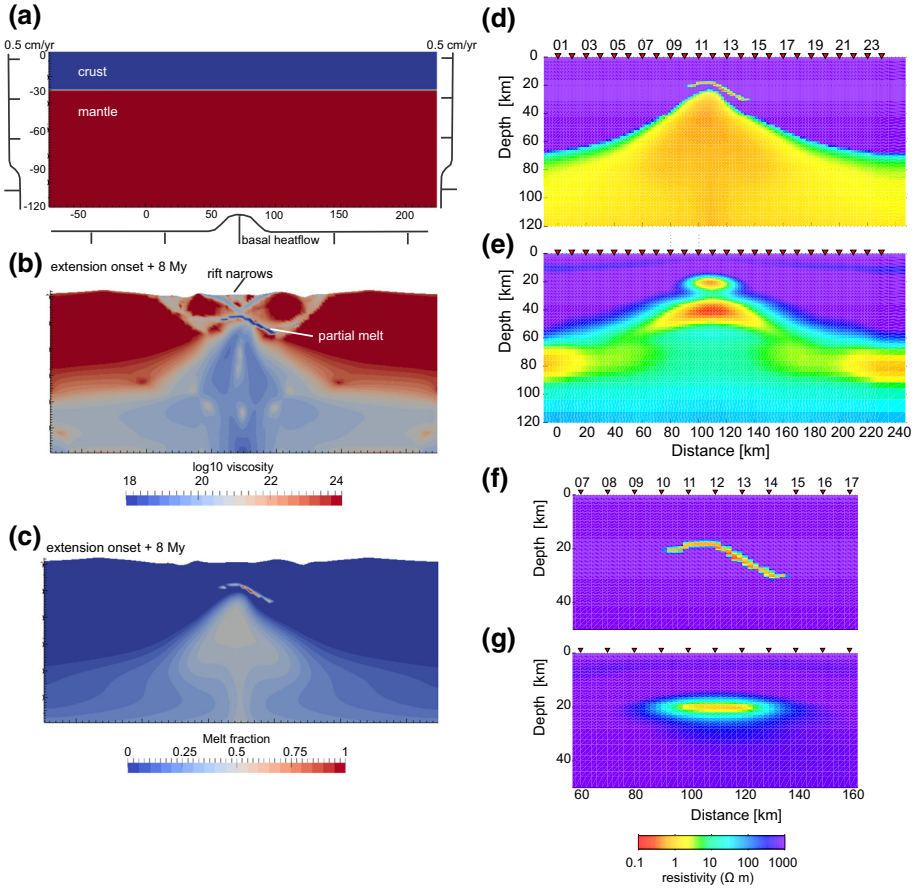

Fig. 7 **a** Set-up of the 2-D thermo-mechanical model with initial crustal thickness of 30 km (*blue*) and mantle (*red*). Elevated heat flow is applied over a small region at the base. After 2 My, extensional boundary conditions are applied as shown. **b** Effective viscosity 8 My after extension starts. A small zone of partial melt has developed at the base of the crust. **c** Partial melt in the thermo-mechanical model after 8 My. **d** Resistivity model calculated from the melt fraction using Hashin–Shtrikman upper bound for a rock matrix of 1000 Ωm and a melt resistivity of 0.2 Ωm. **e** Inversion model for the synthetic MT data obtained from forward modelling model (**d**). **f** Resistivity model of the melt channel without the conductive mantle. **g** Inversion model of the MT data obtained from (**f**)

Melt percentages from the geodynamic model of Kissling and Ellis (2011) can be used to calculate a resistivity model. As part of this review, we have constructed this example to show how geodynamic models that predict partial melt may be used to constrain MT anomalies, and also to show some of the difficulties and ambiguities in this approach. We used the partial melt fraction from Kissling and Ellis (2011) to calculate the bulk resistivity using Hashin–Shtrikman upper bound (for fully interconnected melt) and assuming a rock matrix of 1000 Ωm and a melt resistivity of 0.2 Ωm (Fig. 7d). This resistivity model could then be used as a starting model in an MT inversion or to constrain the results from a MT survey. Here, we calculate synthetic MT responses (0.001–100 s) of this resistivity section at 24 sites with a 10-km spacing. Inversion of the MT data was then used to investigate the resolution of these data for this kind of anomaly. As expected, the narrow melt channel merges with the deeper conductivity anomaly caused by the $\sim$30 % melt in the mantle below (Fig. 7e), but can still be perceived as separate anomaly. The resistor underneath the conductive mantle anomaly shows that the data have no sensitivity below the conductor. A narrow highly conductive melt channel without the deeper anomaly below (Fig. 7f) would also be resolved by the MT data, although the shape of such a feature at a depth of $\sim$20 km cannot be fully recovered and the inversion model shows an elongated conductive "blob". Comparison with the original narrow melt channel highlights the need to understand resolution of MT models in order to interpret and use their results appropriately.

5.5 Multi-inversion Approach to Constrain Mantle Structure

Although not directly applied to geodynamic models, an approach to constrain the bulk mantle structure, temperature and composition with depth was made by Afonso et al. (2013). They use a 3-D multi-observable probabilistic inversion method to calculate lithosphere and mantle structure from the surface to the 410-km discontinuity. Significantly, they used multiple geophysical data including MT (1-D) magnetotelluric data, along with Rayleigh and Love dispersion curves, body-wave tomography, geothermal data, petrological information and gravity (geoid) anomalies. Such an approach could provide important constraints for future geodynamic models at global scale including plates, crustal structure and mantle heterogeneities.

6 Discussion and Conclusions

Our review has shown that while it is still "early days" in linking MT inversions to geodynamic models of lithosphere and mantle, there are a few studies that have attempted to do so where the cause of the MT anomalies is relatively clear, such as in cases where partial melt is present. It is important to note that conductive anomalies in MT models can have a variety of causes, so every anomaly has to be evaluated within its tectonic context. Thorough hypothesis testing of the MT model is necessary to put bounds on the conductors before interpretation. Also, the resolution limits and effect of smoothing in MT models has to be clearly understood so that anomalies are not over- or misinterpreted.

We have highlighted the hierarchy of ways in which MT results can be integrated with geodynamic models. At the simplest level, the interpreted conductivity model is used to define lithological variations, fault locations and/or zones of partial melt while constructing the initial conditions in the geodynamic model; this approach has been used successfully to

pinpoint new zones of mineralization, as discussed in Sect. 5. Alternatively, predictions from geodynamic models for the location and degree of partial melt can be compared to observed MT anomalies (also discussed in the last section). More challenging is when the conductivity model informs melt fraction or fluid content and thus helps to constrain the rheological response to tectonic forcing in geodynamic models. Iterations between predictions from geodynamic and MT models can potentially yield tighter constraints on deformation processes, for example in the case of the conjectured channel flow in the Himalayas.

Most attempts so far, however, have shown that without more detailed studies linking conductivity anomalies to laboratory measurements, it is difficult to use MT results directly in geodynamic models. In attempts to do so, the tectonic context, polymineralic composition of the rocks, sources of fluid generation and possibility of melt must be considered. More laboratory measurements of conductivity (especially under deformation) are needed to constrain the relationships between conductivity, composition, fluid content and other parameters needed by geodynamic modellers.

Despite the difficulties discussed above, some examples of geodynamic models constrained by resistivity models and assuming a straightforward conversion from resistivity to melt have given promising results. Also the growing database of global conductivity data may allow the constraint of global convection models with conductivity data in the (near) future. There is potential in combining the two methods as long as the limitations of each approach are respected.

Acknowledgments We thank Grant Caldwell, Warwick Kissling and Phaedra Upton for discussions and helpful reviews of the draft manuscript. We also thank three anonymous reviewers whose comments significantly improved the manuscript.

References

Afonso JC, Fullea J, Yang Y, Connolly JAD, Jones AG (2013) 3-D multi-observable probabilistic inversion for the compositional and thermal structure of the lithosphere and upper mantle. II: general methodology and resolution analysis. J Geophys Res Solid Earth 118:1650–1676. doi:10.1002/jgrb.50123

Angiboust S, Wolf S, Burov E, Agard Yamato P (2012) Effect of fluid circulation on subduction interface tectonic processes: insights from thermo-mechanical numerical modelling. Earth Planet Sci Lett 358:238–248

Archie GE (1942) The electrical resistivity log as an aid in determining some reservoir characteristics. Trans Am Inst Min Metall Pet Eng 146:54–62

Arora B, Unsworth MJ, Rawat G (2007) Deep resistivity structure of the Northwest Indian Himalaya and its tectonic implications. Geophys Res Lett 34:L04307. doi:10.1029/2006GL029165

Arzi AA (1978) Critical phenomena in the rheology of partially melted rocks. Tectonophysics 44:173–184

Baba K, Chave AD, Evans RL, Hirth G, Mackie RL (2006) Mantle dynamics beneath the East Pacific Rise at 17°S: insights from the Mantle Electromagnetic and Tomography (MELT) experiment. J Geophys Res 111:B02101. doi:10.1029/2004JB003598

Bahr K, Simpson F (2002) Electrical anisotropy below slow and fast-moving plates: Paleoflow in the upper mantle? Science 295:1270–1272

Bahr K, Simpson F (2005) Practical magnetotellurics. Cambridge University Press, Cambridge. ISBN 978-0521817271

Beaumont C, Jamieson RA, Nguyen MH, Lee B (2001) Himalayan tectonics explained by extrusion of a low-viscosity crustal channel coupled to focused surface denudation. Nature 414:738–742

Beaumont C, Jamieson RR, Nguyen MH, Medvedev S (2004) Crustal channel flows: 1. Numerical models with applications to the tectonics of the Himalayan–Tibetan orogen. J Geophys Res 109:B06406. doi:10.1029/2003JB002809

Beaumont C, Nguyen MH, Jamieson RA, Ellis SM (2006) Crustal flow modes in large hot orogens. In: Law RD, Searle MP, Godin L (eds) Channel flow, ductile extrusion and exhumation in continental collision zones. Geological Society of London. Geological Society special publication 268, London, pp 91–145

Becken M, Ritter O, Park SK, Bedrosian PA, Weckmann U, Weber M (2008) A deep crustal fluid channel into the San Andreas Fault system near Parkfield, California. Geophys J Int 173:718–732. doi:10.1111/j.1365-246X.2008.03754.x

Becker TW (2006) On the effect of temperature and strain-rate dependent viscosity on global mantle flow, net rotation, and plate-driving forces. Geophys J Int 167:943–957. doi:10.1111/j.1365-246X.2006.03172.x

Bertrand EA, Caldwell TG, Hill GJ, Wallin EL, Bennie SL, Cozens N, Onacha SA, Ryan GA, Walter C, Zaino A, Wameyo P (2012) Magnetotelluric imaging of upper-crustal convection plumes beneath the Taupo Volcanic Zone, New Zealand. Geophys Res Lett 39(2):L02304. doi:10.1029/2011GL050177

Bibby HM, Caldwell TG, Davey FJ, Webb TH (1995) Geophysical evidence on the structure of the Taupo Volcanic Zone and its hydrothermal circulation. J Volcanol Geotherm Res 68:29–58

Bibby HM, Risk GF, Caldwell TG, Bennie SL (2005) Misinterpretation of electrical resistivity data in geothermal prospecting: a case study from the Taupo Volcanic Zone. In: Proceedings world geothermal congress, Antalya, Turkey

Bittner D, Schmeling H (1995) Numerical modelling of melting processes and induced diapirism in the lower crust. Geophys J Int 123:59–70

Björnsson A, Hersir GP, Björnsson G (1986) The Hengill high-temperature area, S.W. Iceland: regional Geophysical Survey. Geotherm Res Counc Trans 10:205–210

Bollinger L, Henry P, Avouac JP (2006) Mountain building in the Himalaya: thermal and kinematic model from 20 Ma to present. Earth Planet Sci Lett 244:58–71

Brasse H, Eydam D (2008) Electrical conductivity beneath the Bolivian Orocline and its relation to subduction processes at the South American continental margin. J Geophys Res 113:B07109. doi:10.1029/2007JB005142

Brasse H, Lezaeta P, Rath V, Schwalenberg K, Soyer W, Haak V (2002) The Bolivian Altiplano conductivity anomaly. J Geophys Res 107(B5):2096. doi:10.1029/2001JB000391

Bryan CJ, Sherburn S, Bibby HM, Bannister SC, Hurst AW (1999) Shallow seismicity of the central Taupo Volcanic Zone, New Zealand: Its distribution and nature. NZ J Geol Geophys 42:533–542. doi:10.1080/00288306.1999.9514859

Buck WR, Lavier LL (2001) A tale of two kinds of normal fault: the importance of strain weakening in fault development. Geol Soc Lond Spec Publ 187:289–303. doi:10.1144/GSL.SP.2001.187.01.14

Bürgmann R, Dresen G (2008) Rheology of the lower crust and upper mantle: evidence from rock mechanics, geodesy and field observations. Annu Rev Earth Planet Sci 36:531–567

Caricchi L, Gaillard F, Mecklenburgh J, Le Trong E (2011) Experimental determination of electrical conductivity during deformation of melt-bearing olivine aggregates: implications for electrical anisotropy in the oceanic low velocity zone. Earth Planet Sci Lett 302(1):81–94

Carter NL, Tsenn MC (1987) Flow properties of continental lithosphere. Tectonophysics 136:27–63

Chen L, Booker JR, Jones AG, Wu N, Unsworth MJ, Wei W, Tan H (1996) Electrically conductive crust in southern Tibet from INDEPTH magnetotelluric surveying. Science 274:1694–1696

Clark MK, Royden LH (2000) Topographic ooze; building the eastern margin of Tibet by lower crustal flow. Geology 28:703–706

Copley A, McKenzie DP (2007) Models of crustal flow in the India–Asia collision zone. Geophys J Int 169:683–698

Didana YL, Thiel S, Heinson G (2014) Magnetotelluric imaging of upper crustal partial melt at Tendaho graben in Afar, Ethiopia. Geophys Res Lett 41:3089–3095. doi:10.1002/2014GL060000

Duba AG, Shankland TJ (1982) Free carbon & electrical conductivity in the Earth's mantle. Geophys Res Lett 9:1271–1274. doi:10.1029/GL009i011p01271

Eaton DW, Jones AG, Ferguson IJ (2004) Lithospheric anisotropy structure from collocated teleseismic and magnetotelluric observations: great Slave Lake shear zone, Northern Canada. Geophys Res Lett 31:L19614. doi:10.1029/2004GL020939

Eberhart-Phillips D, Bannister SC, Ellis SM (2014) Imaging P and S Attenuation in the Termination Region of the Hikurangi Subduction Zone. Geophys J Int, New Zealand **in review**

Ellis SM, Little TA, Wallace LM, Hacker BR, Buiter SJH (2011) Feedback between rifting and diapirism can exhume ultrahigh-pressure rocks. Earth Planet Sci Lett 311:427–438. doi:10.1016/j.epsl.2011.09.031

Ellis S, Heise W, Kissling W, Villamor P, Schreurs G (2014) The effect of crustal melt on rift dynamics in the central Taupo Volcanic Zone. N Z J Geol Geophys. doi:10.1080/00288306.2014.972961

Evans RL, Tarits P, Chave AD, White A, Heinson G, Filloux JH, Toh H, Seama N, Utada H, Booker JR, Unsworth MJ (1999) Asymmetric electrical structure in the mantle beneath the East Pacific Rise at 17°S. Science 286:752–756

Evans RL, Hirth G, Baba K, Forsyth D, Chave A, Mackie R (2005) Geophysical evidence from the MELT area for compositional controls on oceanic plates. Nature 437:249–252

Gaillard F (2004) Laboratory measurements of electrical conductivity of hydrous and dry silicic melts under pressure. Earth Planet Sci Lett 218:215–228

Gaillard F, Marziano G (2005) Electrical conductivity of magma in the course of crystallization controlled by their residual liquid composition. J Geophys Res 110:B06204. doi:10.1029/2004JB003282

Gaillard F, Malki M, Iacono-Marziano G, Pichavant M, Scaillet B (2008) Carbonatite melts and electrical conductivity in the asthenosphere. Science 322:1363–1365

Gatzemeier A, Moorkamp M (2005) 3D modelling of electrical anisotropy from electromagnetic array data: hypothesis testing for different upper mantle conduction mechanisms. Phys Earth Planet Int 749:225–242

Gerya TV, Meilick FI (2011) Geodynamic regimes of subduction under an active margin: effects of rheological weakening by fluids and melts. J Metamorph Geol 29:7–31. doi:10.1111/j.1525-1314.2010.00904.x

Gerya TV, Yuen DA (2003) Rayleigh–Taylor instabilities from hydration and melting propel 'cold plumes' at subduction zones. Earth Planet Sci Lett 212:47–62

Giordano D, Russell JK, Dingwell DB (2008) Viscosity of magmatic liquids: a model. Earth Planet Sci Lett 271:123–134

Glover PWJ (2010) A generalised Archie's law for n phases. Geophysics 75:E247–E265. doi:10.1190/1.3509781

Glover P, Ádám A (2008) Correlation between crustal high conductivity zones and seismic activity and the role of carbon during shear deformation. J Geophys Res 113:B12210. doi:10.1029/2008JB005804

Glover PWJ, Hole MJ, Pous J (2000) A modified Archie's law for two conducting phases. Earth Planet Sci Lett 180:369–383

Harris N (2007) Channel flow and the Himalayan–Tibetan orogen: a critical review. J Geol Soc 164:511–523

Hashim L, Gaillard F, Champallier R, Le Breton N, Arbaret L, Scaillet B (2013) Experimental assessment of the relationships between electrical resistivity, crustal melting and strain localization beneath the Himalayan–Tibetan Belt. Earth Planet Sci Lett 373:20–30. doi:10.1016/j.epsl.2013.04.026

Hashin Z, Shtrikman S (1962) A variational approach to the theory of effective magnetic permeability of multiphase materials. J Appl Phys 33:3125–3131

Heinson GS, Direen NG, Gill RM (2006) Magnetotelluric evidence for a deep-crustal mineralizing system beneath the Olympic Dam iron oxide copper–gold deposit, southern Australia. Geology 34(7):573–576

Heise W, Caldwell TG, Bibby HM, Brown C (2006) Anisotropy and phase splits in magnetotellurics. Phys Earth Planet Inter 158:107–121

Heise W, Bibby HM, Caldwell TG, Bannister SC, Ogawa Y, Takakura S, Uchida T (2007) Melt distribution beneath a young continental rift: the Taupo Volcanic Zone, New Zealand. Geophys Res Lett 34:L14313. doi:10.1029/2007GL029629

Heise W, Caldwell TG, Bibby HM, Bennie SL (2010) Three-dimensional electrical resistivity image of magma beneath an active continental rift, Taupo Volcanic Zone, New Zealand. Geophys Res Lett 37:L10301. doi:10.1029/2010GL043110

Heise W, Caldwell TG, Hill GJ, Bennie SL, Wallin E, Bertrand EA (2012) Magnetotelluric imaging of fluid processes at the subduction interface of the Hikurangi margin, New Zealand. Geophys Res Lett 39:L04308. doi:10.1029/2011GL050150

Hill GJ, Caldwell TG, Heise W, Chertkoff DG, Bibby HM, Burgess MK, Cull JP, Cas RAF (2009) Distribution of melt beneath Mount St Helens and Mount Adams inferred from magnetotelluric data. Nat Geosci 2:785–789

Hyndman RD, Wang K (1993) Thermal constraints on the zone of major thrust earthquake failure: the Cascadia subduction zone. J Geophys Res 98:2039–2060. doi:10.1029/92JB02279

Itasca Consulting Group (2002) FLAC User's Guide. Itasca Consulting Group Inc, Minneapolis

Jamieson RA, Unsworth MJ, Harris NBW, Rosenberg C, Schulmann K (2011) Crustal melting and the flow of mountains. Elements 7(4):253–260. doi:10.2113/gselements.7.4.253

Ji S, Rondenay S, Mareschal M, Senechal G (1996) Obliquity between seismic and electrical anisotropies as a potential indicator of movement sense for ductile shear zones in the upper mantle. Geology 24:1033–1036

Jiracek GR, Gonzalez VM, Caldwell TG, Wannamaker PE, Kilb D (2007) Seismogenic, electrically conductive, and fluid zones at continental plate boundaries in New Zealand, Himalaya, and California,

USA. In: Okaya DA, Stern TA, Davey FJ (eds) A continental plate boundary: tectonics at South Island, New Zealand. American Geophysical Union: Washington. Geophys Monogr 175: 347–369
Jones AG (2014) Reconciling different equations for proton conduction using the Meyer–Neldel compensation rule. G-Cubed 15:337–349. doi:10.1002/2013GC004911
Jones AG, Lezaeta P, Ferguson IJ, Chave AD, Evans Garcia X, Spratt J (2003) The electrical structure of the Slave craton. Lithos 71:505–527. doi:10.1016/j.lithos.2003.08.001
Kaminski E, Ribe NM, Browaeys JT (2004) D-Rex, a program for calculation of seismic anisotropy due to crystal lattice preferred orientation in the convective upper mantle. Geophys J Int 158(2):744–752
Karato S (2006) Remote sensing of hydrogen in earth's mantle. In: Keppler H, Smyth J (eds) Water in nominally anhydrous minerals. Mineralogical Society of America, Washington, DC, pp 343–375
Karato S (2011) Water distribution across the mantle transition zone and its implications for the global material circulation. Earth Planet Sci Lett 301:413–423
Kelbert A, Schultz A, Egbert G (2009a) Global electromagnetic induction constraints on transition-zone water content variations. Nature 460:1003–1006. doi:10.1038/nature08257
Kelbert A, Egbert G, Schultz A (2009b) Spatial variability of mantle transition zone water content: evidence from global electromagnetic induction data. Abstracts of AGU Fall Meeting, San-Francisco
Keller T, May DA, Kaus BJP (2013) Numerical modelling of magma dynamics coupled to tectonic deformation of lithosphere and crust. Geophys J Int 195:1406–1442
Key K, Constable S, Liu L, Pommier A (2013) Electrical image of passive mantle upwelling beneath the northern East Pacific Rise. Nature 495:499–502
Khan A, Shankland TJ (2012) A geophysical perspective on mantle water content and melting: inverting electromagnetic sounding data using laboratory-based electrical conductivity profiles. Earth Planet Sci Lett. doi:10.1016/j.epsl.2011.11.031
Khan A, Kuvshinov A, Semenov A (2010) On the heterogeneous electrical conductivity structure of the earth's mantle with implications for transition zone water content. J Geophys Res 116:B01103. doi:10.1029/2010JB007458
Kissling W, Ellis SM (2011) Modelling the flow of hydrothermal fluids above an evolving continental rift. Paper no. 86. In: NZ Geothermal Workshop, 21–23 November 2011, Auckland: Workshop programme. Auckland. Proceedings of the New Zealand Geothermal Workshop 33
Klemperer SL (2006) Crustal flow in Tibet: geophysical evidence for the physical state of Tibetan lithosphere, and inferred patterns of active flow. Geol Soc Lond Spec Publ 2006(268):39–70. doi:10.1144/GSL.SP.2006.268.01.03
Kohlstedt D, Mackwell S (1998) Diffusion of hydrogen and intrinsic point defects in olivine. Z Phys Chem 207:147–162
Koons PO, Craw D, Cox SC, Upton P, Templeton AS, Chamberlain CP (1998) Fluid flow during active oblique convergence : a Southern Alps model from mechanical and geochemical observations. Geology 26(2):159–162
Korja T, Engels M, Zhamaletdinov AA, Kovtun AA, Palshin NA, Smirnov MY, Tokarev AD, Asming VE, Vanyan LL, Vardaniants IL, BEAR Working Group (2002) Crustal conductivity in Fennoscandia—a compilation of a database on crustal conductance in the Fennoscandian Shield. Earth Planets Space 54:535–558
Kreutzmann A, Schmeling H, Junge A, Ruedas T, Marquart G, Bjarnason IT (2004) Temperature and melting of a ridge-centered plume with application to Iceland, part II: predictions for electromagnetic and seismic observables. Geophys J Int 159:1097–1111
Kuvshinov A (2011) Deep electromagnetic studies from land, sea, and space: progress status in the past 10 years. Surv Geophys. doi:10.1007/s10712-011-9118-2
Kuvshinov A, Utada H, Avdeev DB, Koyama T (2005) 3-D modelling and analysis of Dst C-responses in the North Pacific Ocean region, revisited. Geophys J Int 160:505–526
Laumonier M, Gaillard F, Sifré D (2014) The effect of pressure and water concentration on the electrical conductivity of Dacitic melts: implication for magnetotelluric imaging in subduction areas. Chem Geol. doi:10.1016/j.chemgeo.2014.09.019
Lemmonier C, Marquis G, Perrier F, Avouac JP, Chitrakar G, Kafle B, Sapkota S, Gautam U, Tiwari D, Bano M (1999) Electrical structure of the Himalaya of Central Nepal: high conductivity around the mid-crustal ramp along the MHT. Geophys Res Lett 26:3261–3264
Li S, Unsworth MJ, Booker JR, Wei W, Tan H, Jones AG (2003) Partial melt or aqueous fluid in the mid-crust of southern Tibet? Constraints from INDEPTH magnetotelluric data. Geophys J Int 153:289–304
Litchfield N, Van Dissen R, Sutherland R, Barnes P, Cox S, Norris R, Beavan RJ, Langridge R, Villamor P, Berryman K (2014) A model of active faulting in New Zealand. N Z J Geol Geophys 1:1–25

Liu L, Wan C, Zhao C, Zhao Y (2011) Geodynamic constraints on orebody localization in the Anqing orefield, China: computational modeling and facilitating predictive exploration of deep deposits. Ore Geol Rev 43:249–263

Liu J, Karrech A, Regenauer-Lieb K (2014) Combined mechanical and melting damage model for geomaterials. Geophys J Int 198:1319–1328

McGary RS, Evans RL, Wannamaker PE, Elsenbeck J, Rondenay S (2014) Subducting slab to surface pathway for melt and fluids beneath Mount Rainier. Nature 511:338–341

Meqbel NM, Egbert GD, Wannamaker PE, Kelbert A, Schultz A (2014) Deep electrical resistivity structure of the northwestern U.S. derived from 3-D inversion of USArray magnetotelluric data. Earth Planet Sci Lett. doi:10.1016/j.epsl.2013.12.026

Miyazaki T, Sueyoshi K, Hiraga T (2013) Olivine crystals align during diffusion creep of Earth's upper mantle. Nature 502:321–326

Naif S, Key K, Constable S, Evans RL (2013) Melt-rich channel observed at the lithosphere–asthenosphere boundary. Nature 495:356–359

Nelson KD et al (1996) Partially molten middle crust beneath southern Tibet: synthesis of project INDEPTH results. Science 274:1684–1688

Nicol A, Wallace LM (2007) Temporal stability of deformation rates : comparison of geological and geodetic observations, Hikurangi subduction margin, New Zealand. Earth Planet Sci Lett 258(3/4):397–413. doi:10.1016/j.epsl.2007.03.039

Norris RJ, Koons PO, Cooper AF (1990) The obliquely-convergent plate boundary in the South Island of New Zealand: implications for ancient collision zones. J Struct Geol 12:715–725

Ogawa Y, Honkura Y (2004) Mid-crustal electrical conductors and their correlations to seismicity and deformation at Itoigawa-Shizuoka Tectonic Line, Central Japan. Earth Planets Space 56:1285–1291

Pek J, Santos FAM (2006) Magnetotelluric inversion for anisotropic conductivities in layered media. Phys Earth Planet Int 158:139–158

Pellerin L, Johnston JM, Hohmann GW (1996) A numerical evaluation of electromagnetic methods in geothermal exploration. Geophysics 61:121–130

Poe BT, Romano C, Varchi V, Misiti V, Scarlato P (2008) Electrical conductivity of a phonotephrite from Mt. Vesuvius: the importance of chemical composition on the electrical conductivity of silicate melts. Chem Geol 256:192–201

Poe B, Romano C, Nestola F, Smyth JR (2010) Electrical conductivity anisotropy of dry and hydrous olivine at 8 GPa. Phys Earth Planet Inter 181:103–111

Pommier A (2013) Interpretation of magnetotelluric results using laboratory measurements. Surv Geophys. doi:10.1007/s10712-013-9226-2

Pommier A, LeTrong E (2011) "SIGMELTS": a webportal for electrical conductivity calculations in geosciences. Comput Geosci 37:1450–1459

Pommier A, Gaillard F, Pichavant M, Scaillet B (2008) Laboratory measurements of electrical conductivities of hydrous and dry Mount Vesuvius melts under pressure. J Geophys Res. doi:10.1029/2007jb005269

Pommier A, Evans RL, Key K, Tyburczy J, Mackwell S, Elsenbeck J (2013) Prediction of silicate melt viscosity from electrical conductivity: a model and its geophysical implications. G-Cubed. doi:10.1002/2012GC004467

Pous J, Muñoz JA, Ledo JJ, Liesa M (1995) Partial melting of subducted continental lower crust in the Pyrenees. J Geol Soc (London) 152:217–220

Pous J, Muñoz G, Heise W, Melgarejo JC, Quesada C (2004) Electromagnetic imaging of Variscan crustal structures in SW Iberia: the role of interconnected graphite. Earth Planet Sci Lett 217:435–450

Quinquis MET, Buiter SJH (2014) Testing the effects of basic numerical implementations of water migration on models of subduction dynamics. Solid Earth 5:537–555. doi:10.5194/se-5-537-2014

Rey PF, Teyssier C, Whitney DL (2009) Extension rates, crustal melting, and core complex dynamics. Geology 37:391–394

Rippe D, Unsworth MJ (2010) Quantifying crustal flow in Tibet with magnetotelluric data. Phys Earth Planet Inter 179:107–121. doi:10.1016/j.pepi.2010.01.009

Rippe D, Unsworth MJ, Currie CA (2013) Magnetotelluric constraints on the fluid content in the upper mantle beneath the southern Canadian Cordillera: implications for rheology. J Geophys Res 118(10):5601–5624

Roberts JJ, Tyburczy JA (1999) Partial-melt electrical conductivity: influence of melt composition. J Geophys Res 104:7055–7065

Rodi WL, Mackie RL (2012) The inverse problem. In: Chave A, Jones AG, Mackie RL, Rodi WL (eds) The magnetotelluric method—theory and practice, vol 8. Cambridge University Press, New York. ISBN 9780521819275

Rosenberg CL, Handy MR (2005) Experimental deformation of partially melted granite revisited: implications for the continental crust. J Metamorph Geol 23:19–28
Rosenberg CL, Medvedev S, Handy M (2007) On the effects of melting on continental deformation and faulting. In: Handy M, Hirth G, Hovius N (eds) Tectonic faults: agents of change on a dynamic earth. In: Dahlem Workshop Report 95, MIT Press, pp 357–402
Ruedas T, Schmeling H, Marquart G, Kreutzmann A, Junge A (2004) Dynamics and melting of a ridge-centered plume with application to Iceland, part I: evolution and crust production. Geophys J Int 158:729–743
Saffer DM, Lockner DA, McKiernan A (2012) Effects of smectite to illite transformation on the frictional strength and sliding stability of intact marine mudstones. Geophys Res Lett 39:L11304. doi:10.1029/2012GL051761
Schäfer A, Houpt L, Brasse H, Hoffmann N, EMTESZ Working Group (2011) The North German conductivity anomaly revisited. Geophys J Int 187:85–98. doi:10.1111/j.1365-246X.2011.05145.x
Schilling FR, Partzsch GM (2001) Quantifying partial melt fraction in the crust beneath the central Andes and the Tibetan Plateau. Phys Chem Earth 26:239–246
Schilling FR, Partzsch GM, Brasse H, Schwarz G (1997) Partial melting below the magmatic arc in the central Andes deduced from geoelectromagnetic field experiments and laboratory data. Phys Earth Planet Inter 103:17–31
Schmeling H (2010) Dynamics models of continental rifting with melt generation. Tectonophysics 480:33–47
Selway KM (2013) On the causes of electrical conductivity in stable lithosphere. Surv Geophys 35:219–257. doi:10.1007/s10712-013-9235-1
Semenov A, Kuvshinov A (2012) Global 3-D imaging of mantle conductivity based on inversion of observatory C-responses—II. Data analysis and results. Geophys J Int. doi:10.1111/j.1365-246X.2012.05665.x
Simpson F (2001) Resistance to mantle flow inferred from the electromagnetic strike of the Australian upper mantle. Nature 412:632–635
Simpson F (2013) Distribution functions for anisotropic electrical resistivities due to hydrogen diffusivity in aligned peridotite and their application to the lithosphere–asthenosphere boundary. Tectonophysics 592:31–38
Siripunvaraporn W, Egbert G (2009) WSINV3DMT: vertical magnetic field transfer function inversion and parallel implementation. Phys Earth Planet 173(3–4):317–329
Smith JT, Hoversten GM, Gasperikova E, Morrison HF (1999) Sharp boundary inversion of two-dimensional magnetotelluric data. Geophys Prospect 47:469–486
Spratt JE, Jones AG, Nelson KD, Unsworth MJ, The INDEPTH MT Team (2005) Crustal structure of the India–Asia collision zone, southern Tibet, from INDEPTH MT investigations. Earth Planet Sci Lett 150:227–237
Stanley WD, Mooney WD, Fuis GS (1990) Deep crustal structure of the Cascade range and surrounding regions from seismic refraction and magnetotelluric data. J Geophys Res 95:19419–19438
ten Grotenhuis SM, Drury MR, Peach CJ, Spiers CJ (2004) Electrical properties of fine-grained olivine: evidence for grain boundary transport. J Geophys Res 109:B06203. doi:10.1029/2003JB002799
Tommasi A, Mainprice D, Canova G, Chastel Y (2000) Viscoplastic self-consistent and equilibrium-based modeling of olivine lattice preferred orientations: implications for the upper mantle seismic anisotropy. J Geophys Res 105(B4):7893–7908. doi:10.1029/1999JB900411
Toomey DR, Wilcock WSD, Conder JA, Forsyth DW, Blundy JD, Parmentier EM, Hammond WC (2002) Asymmetric mantle dynamics in the MELT region of the East Pacific Rise. Earth Planet Sci Lett 200:287–295
Toussaint G, Burov E, Avouac J-P (2004) Tectonic evolution of a continental collision zone: a thermomechanical numerical model. Tectonics 23. TC001604
Tyburczy J, Waff HS (1983) Electrical conductivity of molten basalt and andesite to 25 kilobars pressure: geophysical significance and implications for the charge transport and melt structure. J Geophys Res 88:2413–2430
Unsworth MJ (2010) Magnetotelluric studies of continent–continent collisions. Surv Geophys 31:137–161
Unsworth MJ, Rondenay S (2013) Mapping the distribution of fluids in the crust and lithospheric mantle utilizing geophysical methods. In: Harlov DE, Austrheim H (eds) Metasomatism and the chemical transformation of rock: the role of fluids in crustal and upper mantle processes series, Lecture notes in earth system sciences. Springer-Verlag, Berlin, pp 535–598
Unsworth MJ, Wei W, Jones AG, Li S, Bedrosian PA, Booker JR, Jin S, Deng M (2004) Crustal and upper mantle structure of Northern Tibet imaged with magnetotelluric data. J Geophys Res. doi:10.1029/2002JB002305

Unsworth MJ, Jones AG, Wei W, Marquis G, Gokarn S, Spratt JE, the INDEPTH-MT team (2005) Crustal rheology of the Himalaya and Southern Tibet inferred from magnetotelluric data. Nature 438:78–81. doi:10.1038/nature04154

Upton P (1998) Modelling localization of deformation and fluid flow in a compressional orogen : implications for the Southern Alps of New Zealand. Am J Sci 298(4):296–323

Upton P, Craw D (2008) Modelling the role of graphite in development of a mineralised mid-crustal shear zone, Macraes mine, New Zealand. Earth Planet Sci Lett 266(3/4):245–255. doi:10.1016/j.epsl.2007.10.048

Upton P, Caldwell TG, Chamberlain CP, Craw D, James Z, Jiracek GJ, Koons PO, Wannamaker PE (2000) Fluids in a backthrust regime (Southern Alps, New Zealand). J Geochem Explor 69(70):517–521

Ussher G, Harvey C, Johnstone R, Anderson E (2000) Understanding resistivities observed in Geothermal Systems. In: Proceedings World Geothermal Congress 2000, Kyushu-Tohoku, Japan

Villamor P, Berryman KR (2006) Evolution of the southern termination of the Taupo Rift, New Zealand. N Z J Geol Geophys 49:23–37

Waff HS (1974) Theoretical consideration of electrical conductivity in a partially molten mantle and implications for geothermometry. J Geophys Res 79:4003–4010

Waff HS, Weill DF (1975) Electrical conductivity of magmatic liquids: effects of temperature, oxygen fugacity and composition. Earth Planet Sci Lett 28:254–260

Wang D, Mookherjee M, Xu YS, Karato S (2006) The effect of hydrogen on the electrical conductivity in olivine. Nature 443:977–980

Wang X, Zhang G, Fang H, Luo W, Zhang W, Zhong Q, Cai X, Luo H (2013) Crust and upper mantle resistivity structure at middle section of Longmenshan, eastern Tibetan plateau. Tectonophysics. doi:10.1016/j.tecto.2013.09.011

Wannamaker PE, Jiracek GR, Stodt JA, Caldwell TG, Gonzalez VM, McKnight JD, Porter AD (2002) Fluid generation and pathways beneath an active compressional orogen, the New Zealand Southern Alps, inferred from Magnetotellurics (MT) data. J Geophys Res 107(ETG 6):1–20

Wannamaker PE, Caldwell TG, Jiracek GR, Maris V, Hill GJ, Ogawa Y, Bibby HM, Bennie SL, Heise W (2009) Fluid and deformation regime of an advancing subduction system at Marlborough, New Zealand. Nature. doi:10.1038/nature08204

Wilson CJN, Houghton BF, McWilliams MO, Lanphere MA, Weaver SD, Briggs RM (1995) Volcanic and structural evolution of Taupo Volcanic Zone, New Zealand: a review. J Volcanol Geotherm Res 68:1–28

Ye G, Jin S, Wei W, Unsworth MJ (2007) Research of the conductive structure of crust and the upper mantle beneath the South-Central Tibetan Plateau. J China Univ Geosci 18:334–343

Yoshino T, Matsuzaki T, Shatskiy A, Katsura T (2009) The effect of water on the electrical conductivity of olivine aggregates and its implications for the electrical structure of the upper mantle. Earth Planet Sci Lett 288:291–300

Zhao G, Unsworth MJ, Zhan Y, Wang L, Chen X, Jones A, Tang J, Xiao Q, Wang J, Cai J, Li T, Wang Y, Zhang J (2012) Crustal structure and rheology of the Longmenshan and Wenchuan Mw 7.9 earthquake epicentral area from magnetotelluric data. Geology 40:1139–1142. doi:10.1130/G33703.1